Fabrication and Analysis of a YAG Silica Fiber

Arian Chimenson
arian.chimenson@student.tabyenskilda.se

under the direction of
Dr. Clarissa Harvey
Department of Applied Physics
KTH Royal Institute of Technology

Research Academy for Young Scientists
July 13, 2022

Abstract

Optical fibers have a wide variety of applications, ranging from telecommunication cables to medicine and astronomy. The aim of this study was to fabricate a YAG silicate fiber with an increased content of YAG in the fiber's core in order to study its structural properties, elemental composition, and optical properties. By fabricating the fiber through the molten-core method, the elemental content of silicon in the core was estimated to be $8.5 \pm 2.6\,\mathrm{wt\%}$. It was concluded, that the method used in this study is feasible for fabricating Nd:YAG optical fibers with a higher purity of the core than in previous studies. However, deviations of optical measurements for the angular acceptance of the fiber from theory and Gaussian beam models, indicates that the underlying method was inaccurate. Thus, future studies need to be conducted in order to improve the accuracy of the optical measurements, the fiber's structure and the purity of the fiber's core as well as to study novel combinations of materials with similar thermal properties and semiconductive crystalline structure.

Acknowledgements

I would like to express my deepest gratitude to my supervisor, Dr. Clarissa Harvey, for the invaluable and continuous assistance during this project. I would also like to thank everyone at KTH Laser physics group for welcoming me to AlbaNova and introducing me to the facilities as well as my lab partner, Lovisa Diding, for the assistance in the practical and computational aspects of this project. I also express my gratitude to Rays - for excellence as well and our collaborative partners Bejerstiftelsen and Ekmanstiftelserna without whom the completion of this project would not have been possible. Finally, I would like to thank Viktor Sundström, Erik Eldh, and Tuva Källberg for their indispensable assistance during the writing process.

Contents

1 Introduction

Optical fibers have a wide range of applications, such as in telecommunication cables, medical sensors, and power transmission. The main advantages of optical fibers are their mechanical flexibility and lower attenuation compared to coaxial electrical cables [1].

1.1 Material and Structural Properties of an Optical Fiber

As seen in Figure 1, an optical fiber is cylindrical and consists of three circular layers: a core, a cladding, and a coating [1]. Light is launched into the core by a laser and propagates predominantly in the core. Because of low propagation losses, optical intensity can be maintained over longer distances. [1].

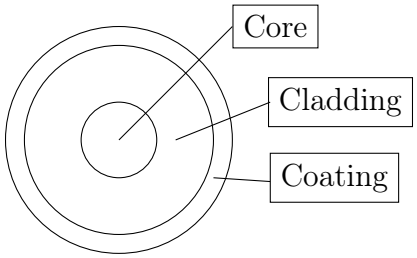

Figure 1: An illustration of the cross section of an optical fiber.

The core has a higher refractive index than the cladding. Various dopants can be used, to alter the refractive indices of the layers.

In this case, the fabricated fiber was a step-index fiber, where the refractive index is constant within the core and the cladding [1]. The core consisted of YAG (Yttrium aluminum garnet, $Y_3Al_5O_{12}$) doped with 1 wt% (weight percent) neodymium (Nd) and the cladding consisted of silica (SiO_2).

1.2 Geometrical Optics of an Optical Fiber

Geometrical optics is a simplified model of optics, where the main premise is that light rays propagate in a straight-line path if the refractive index is constant. The refractive index of a medium, n, is defined as $n = \frac{c}{v}$, where c is the speed of light in vacuum, and

v the speed of light in the medium [2]. When the refractive index changes, as the light ray passes the interface (boundary) between two media, the ray will curve as described by Snell's law [3, 2]. Snell's law states that the incident ray, the refracted ray, and the normal perpendicular to the interface will all lie in the same plane, as seen in Figure 2. The angle of the incident ray, θ_1 and the angle of refracted ray, θ_2 are related through

$$\frac{\sin\theta_1}{\sin\theta_2} = \frac{n_2}{n_1} = \frac{v_1}{v_2}, \tag{1}$$

where n_1 and n_2 are the refractive indices of each medium, and v_1 and v_2 the speed of light in each respective medium.[4]

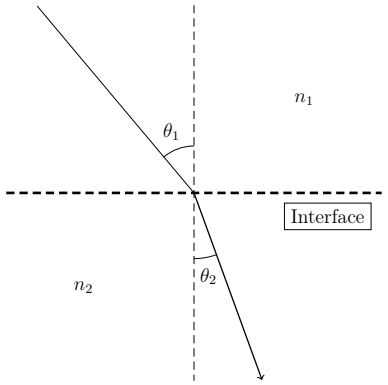

Figure 2: Refraction of a light ray at the interface between two media of different refractive indices.

When light travels in a medium of refractive index n_s to medium of refractive index n_f, total internal reflection can occur, if the incident angle is above a certain critical angle [5],

$$\theta_c = \arcsin\frac{n_f}{n_s}. \tag{2}$$

There is however another condition for total internal reflection in an optical fiber. Light will only propagate if the incident angle of the ray entering the core of the fiber is less than an acceptance angle θ_α. The numerical aperture, A_N, is a measure of the angular

acceptance of a fiber and is defined as

$$A_N = n \sin \theta_\alpha = \sqrt{n_{core}^2 - n_{cladding}^2}, \tag{3}$$

where n_{core}, n, $n_{cladding}$ are the refractive indices of the core, surrounding medium, and cladding respectively [6]. The numerical aperture can also be used to define the normalized frequency of light, the V number, as

$$V = \frac{2\pi}{\lambda} a A_N = \frac{2\pi}{\lambda} a \sqrt{n_{core}^2 - n_{cladding}^2}, \tag{4}$$

where λ is the vacuum wavelength of the light and a is the radius of the fiber core [7].

1.3 Electromagnetic Properties of an Optical Fiber

In 1865, James Clerk Maxwell effectively showed that light is an electromagnetic wave, a coupled magnetic and electric field, propagating through space at the speed of light, $c \approx 299\ 792\ 458\ \mathrm{m\,s^{-1}}$ as described by Maxwell's equations.

Electromagnetic waves in an optical medium often propagate in different modes, i.e. with a certain field pattern and a changing phase. Using Maxwell's equations, the electromagnetic wave equation can be derived from modes can be obtained. The number of modes, N_M can be approximated using the V-number from equation (4) [7]. If $V < 2.405$, the medium contains a single mode, otherwise N_M can be approximated with

$$N_M \approx \frac{V^2}{2} [7]. \tag{5}$$

If an electromagnetic wave is emitted by a laser it is, in most scenarios, a Gaussian beam, which can be used a as more sophisticated model of optics than the geometrical. The electric field for a Gaussian beam, $\mathbf{E}(r, z)$, is given by

$$\mathbf{E}(r, z) = E_0 \, \hat{\mathbf{x}} \, \frac{w_0}{w(z)} \exp\left(\frac{-r^2}{w(z)^2}\right) \exp\left(-i\left(kz + k\frac{r^2}{2R(z)} - \psi(z)\right)\right), \tag{6}$$

where r is the distance from the center of the beam's cross section, z, is the distance from the beam's waist (the location where the beam radius has a minimum), $k = \frac{2\pi n}{\lambda}$ is the wave number (the spatial wave frequency), $E_0 = E(0,0)$ is the value of the electric field at the origin, $w(z)$ the beam radius as a function of z, $w_0 = w(0)$ the waist radius, $R(z)$ the radius of curvature of the beam's wavefronts as a function of z, and $\psi(z)$ the Gouy phase as a function of z, which is an additional phase shift acquired by a converging wave passing though a focus [8].

The intensity of the Gaussian beam, $I(r,z)$, follows a Gaussian distribution such that

$$I(r,z) = I_0 \left(\frac{w_0}{w(z)}\right)^2 \exp\left(\frac{-2r^2}{w(z)^2}\right), \tag{7}$$

where $I_0 = I(0,0)$ is the intensity of the beam at the origin [9]. Furthermore, the half-angle divergence of a Gaussian beam, θ_d, can be defined as

$$\theta_d = \frac{\lambda}{\pi w_o}, \tag{8}$$

which is a property of the beams expansion from its waist [8].

1.4 Interaction of the Fiber with Different Wavelengths

Light of a certain wavelength interacting with common materials in a medium, such as an optical fiber, usually results in transmission, absorption, emission. In the case of pure silica and YAG, light is is usually transmitted at most wavelengths between 250 nm to 5000 nm [10, 11, 12]. However dopped YAG with for instance Neodymium will have a different transmission spectrum [11] — wavelengths of about 730 nm and 800 nm are usually absorbed [13]. However, light at a wavelength like 808 nm, will result in emission of certain wavelengths by the core through amplified spontaneous emission (ASE) [14]. ASE is a result of spontaneous emission, amplified by stimulated emission [14]. Spontaneous emission occurs when a quantum mechanical system, such as an atom or an ion, transits

from an excited higher energy state to a lower energy state and the energy is emitted in the form of a photon [15]. The spontaneous emission occurs in the fiber's core and the emission is amplified through stimulated emission, which mean that an incoming photon de-excites electrons [16]. For stimulated emission, the released photon will have the same frequency, polarization, and direction as the incident photon [16]. For ASE to take place, a population inversion (more electrons are in a higher energy state than in a lower) is required [17] and is created by optical pumping of the fiber's core, i.e. energy transfer from a light source to excite the electrons in the fiber's core [18].

In the case of Nd:YAG (neodymium-doped YAG), ASE occurs when light of a certain wavelength like 808 nm interacts with the material and certain wavelengths of light are emitted. The usual emitted wavelengths characteristic to Nd:YAG are approximately 946 nm, 1064 nm, and 1338 nm [19].

1.5 Fabrication of an Optical Fiber

There are multiple methods for fabricating fibers. One is the molten core method, where the fiber is pulled from a preform by a fiber-drawing tower [20]. A preform is a cylindrical rod that has the same composition of materials in the core and the cladding as the desired fiber, but has a greater diameter and length [21]. The fiber-drawing tower contains a furnace, which heats up the bottom of the preform rod in order for a thin fiber to be pulled out from the bottom of the preform [20], as seen in Figure 3. This process is carried out in vacuum to avoid air bubbles in the fiber [20].

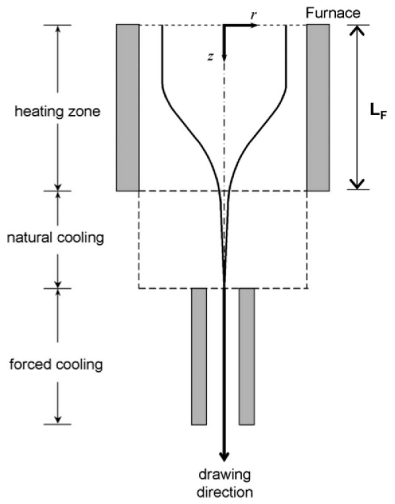

Figure 3: An illustration of the pulling of the fiber from the preform [22].

As the fiber is cooled in a separate chamber to become a solid [20] a coating is applied [23]. It is wound up on a spinning spool in order to keep the fiber diameter constant along the whole fiber, the pulling speed is adjusted with an automatic feedback system [20]. A constant fiber diameter also leads to a more constant core diameter, which is of importance because it affects the number of modes in the fiber and the allowed angle of incidence [21].

1.6 Thermal Aspects of Fiber Fabrication

During the fabrication fiber in a drawing-tower, the preform is heated to a temperature such that the viscosity of the materials is in a suitable range for pulling. The melting point of silica is 1710 °C [24] and the melting point of YAG is 1940 °C [25]. The relatively close melting points allows for both materials to be in viscous, liquid, form during the drawing process [26]. However, the characteristics of the phase transition of silica makes it more viscous than YAG in a liquid state [26, 27], which allows the for the drawing process to proceed with less diffusion.

Both the material in the core and in the cladding undergoes thermal expansion during the heating phase. In the case of an optical fiber, thermal expansion of the core's and cladding's volume occurs in all directions as temperature increases. The coefficient

of thermal expansion governs how much the volume expands with every increase in temperature. The coefficient of thermal expansion for silica is $5.6 \cdot 10^{-7}$K [28] and for YAG it is $7.8 \cdot 10^{-6}$ K [25]. A greater thermal expansion coefficient also implies faster thermal reduction of the volume, and thus in theory, thermal expansion could lead to a non-uniform core-structure and composition of elements in the core. Furthermore, since the shape would be altered, it would affect the fibers optical properties by changing the angle of incidence and potentially leading to the light in the fiber and hence transmission losses.

1.7 Scanning Electron Microscope

A Scanning Electron Microscope (SEM) is designed for studying the surfaces of objects and uses a shorter wavelength than optical microscopes, allowing for higher resolution [29]. With electromagnetic lenses and apertures a focused beam of electrons is used to scan the surface of the sample [29]. The electrons interact with the sample by emitting secondary electrons (i.e. electrons with energies below 50 eV), backscattered electrons, auger electrons, and X-rays [30]. Various detectors are used to collect and process these signals in order to form an image of the studied sample's surface [30].

It is important that the beam is in a vacuum, because the electrons would otherwise get absorbed or scatter in the atmosphere. Furthermore, the surface of the studied sample should be electrically conductive and is therefore often covered by a thin layer of a conductive material, such as graphite [29].

1.8 Energy-dispersive X-ray Spectroscopy

An energy-dispersive X-ray spectroscopy (EDS) is a technique used to analyze the composition of elements in a sample [30]. EDS relies on Moseley's law, which states that there is correlation between the frequency of x-ray and the atomic number of an element, more precisely that

$$\sqrt{v} \propto Z \tag{9}$$

where v is the frequency of the X-ray and Z the atomic number of the element [31].

A sample studied through EDS contains unexcited ground state electrons [32]. By emitting electrons focused on a sample, the incident beam excites an electron in an inner shell of an atom, ejecting it [32]. An electron from an outer, higher-energy, shell fills this void and the energy difference between the lower and higher energy shell is emitted in the form of an X-ray [32]. This phenomena is called the Auger effect [33]. As the difference in energy is characteristic to the specific element, its occurrence and content in the studied sample can be determined [30].

1.9 Previous Research on YAG-derived Optical Fibers

The most common type of optical fiber consists of silica (SiO_2) in both the core and the cladding [34]. For achieving a refractive index difference between the core and the cladding, usually dopants such as germanium dioxide (GeO_2) and phosphorus pentoxide (P_2O_5) are used for increasing the refractive index of the core [23]. For decreasing the refractive index of cladding, dopants such as boron and fluorine are used [23].

Extensive research has been conducted on the feasibility of different crystalline compounds as a material for the core, usually semiconductors in crystalline form [35]. However, few studies have been conducted on the fabrication and viability of YAG as material for the fiber's core with one of the reasons being the different thermal expansions of the materials [26]. Prior attempts to fabricate a YAG silicate fiber with the molten core method have resulted in a mixed core composition of mainly yttrium aluminosilicate composition, meaning a significant elemental content of the silicon from the cladding in the fiber's core with an estimate of 75.3 wt% [26, 36]. Hence, prior research has been done on mainly YAG-derived fibers with a mixed elemental composition of the core, often dominated by silicon from the cladding [37, 38].

1.10 Aim of Study

The aim of this study was to fabricate a YAG silicate optical fiber with an increased content of YAG in the fiber's core in order to study its structural properties, elemental composition, and optical angular acceptance by comparing the the results obtained from models based on geometrical optics and Gaussian beam theory.

2 Method

A YAG silicate fiber was fabricated with the molten core method. The structural properties and materials properties of multiple samples of the fiber were studied by examining its structure, estimating its dimensions, and measuring the content of the elements in silica and Nd:YAG. Optical measurements were conducted by measuring the angular acceptance of the fiber using models based on geometrical optics and Gaussian beam theory as well as by optically measuring the transmission and emission spectra of the fiber.

2.1 Fabrication of the Fiber

The fiber was fabricated from a preform consisting of a 12 cm silica capillary with two 2 cm 1 wt% Nd-doped YAG-rods in the middle of the cylindrical capillary. It was 12 cm in total with an outer diameter of 6 mm and the inner diameter of 1 mm. The preform was fabricated by placing the Nd:YAG rods in the silica capillary and heating it to 2000°C.

A fiber drawing-tower was used and in the process, the bottom of the preform was heated to approximately 2000 °C in order to pull the fiber. A UV-curable polymer coating was applied and approximately 10 m of YAG silicate fiber was wound up on a spinning spool.

2.2 Micro- and Nanoanalysis of the Fabricated Fiber

The obtained optical fiber was cut into 1 m to 2 m samples with pliers. The coating of each sample was dissolved in acetone in order to examine it under a microscope. Both the side-view and the cross-section were inspected for structural irregularities, such as holes and air bubbles in core, where no YAG was present. Several samples of the fiber with as few imperfections as possible and with YAG in the core were chosen, since these imperfections could lead to light scattering and additional transmission losses. Multiples measurements were conducted with the samples in order to estimate the diameter of fiber's cross section.

The structure of the samples were then examined with a SEM in order to further study irregularities in the fiber. At the same time, an EDS was carried out in order to estimate the occurrence and content of the elements aluminum (Al), oxygen (O), silicon (Si), yttrium (Yt), and neodymium (Nd) in the fiber. If the elements specific to the compounds in the core and the cladding were present in another layer, it could be a consequence of thermal expansion, diffusion, various mechanical tensions, and other possible imperfections of the fabrication process.

2.3 Measurements of the Optical Properties of the Fiber

In order to prepare for optical measurements of the fiber, the cross sections of the samples without holes and with a core where YAG was present were made as smooth as possible. The ends of the fiber were cleaved and a portable fiber microscope was used to examine the surface for tensions, scratches, and other mechanical damage. Both ends of the samples were polished with abrasive paper. When both ends of the samples were deemed polished with no visible irregularities, they were deemed ready for optical measurements.

2.3.1 Experimental Setup

As seen in Figure 4, the experimental configuration consisted of a White-ligt WhiteLase SC480 Ultra High-Power Supercontinuum Fiber Laser for conducting the measurements of the numerical aperture connected to a 16x 11 mm collimating lens with a single-mode optical fiber (SMF) with an 8 µm core. The collimating lens was used to narrow the beam going through an aperture to augment the beam when entering a 2.8 mm 60x focusing lens which was used to match the beam diameter to the fiber's core diameter. The focusing lens and the the fiber under test were both mounted on separate translation stage in order to align the fiber and the lens in all three directions.

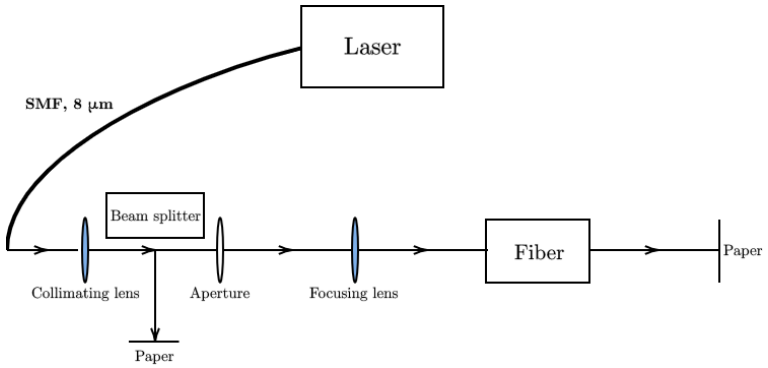

Figure 4: An schematic illustration of the optical configuration.

A rectangular piece of paper was put in front of the other of the fiber though which light was leaving the fiber. A CCD-camera was mounted on a translation stage in front of the other end of fiber in order to take pictures of the beam sport during the measurements.

2.3.2 Angular Acceptance, V-number and the Number of Modes

The optical configuration described was used to measure the value of the numerical aperture, the V-number and the number of modes. By aligning the laser beam with the beam splitter that translated the front end of the fiber, it was ensured that the light went in to the core. When alignment was done, the beam splitter was removed and the beam focused on a piece of rectangular white paper. A photo of the spot from the laser beam was taken, by the CCD-camera mounted on the translation stage pointed at the opposite side of the

piece of paper. Note that the exposure of the CCD-camera was set to the minimal value so only the spot from the beam would be visible. By adjusting the translation stage, the distance of the camera was increased and another picture was taken. This process was iterated for every sample and in case of the the spot not being visible, the exposure of the CCD-camera was increased to such a value that surrounding light, except for the spot from the beam, could not be seen through the camera.

The images for each sample were analyzed using the image processing software Fiji based on the library ImageJ. The Gaussian intensity profile of the spot from the laser beam was measured.

Some small deviations arose when the visibility of the spot was lower or light from other sources than the laser was captured by the camera, which led to noise being observed on the graph of the intensity distribution of the beam at a certain distance from the beam waist. The values for each sample were extracted. For each data set corresponding to a certain distance of the translation stage from the piece of paper, a Gaussian function was fitted to the values. From the Gaussian functions for each data set, the the radius of the laser beam was extracted to a single set of data and plotted as a function a of the distance from the beam waist. The values followed a linear trend and thus a linear function was fitted, which represented the radius of the beam as a function of distance from the beam waist. The acceptance angle, θ_α, was calculated with

$$\theta_\alpha = \arctan\left(\frac{\Delta y}{\Delta x}\right) \tag{10}$$

where Δy is the the radius of the beam at a certain distance Δx from the beam waist. This ratio is constant for a linear dependency and is known as the slope, thus the tangent of the slope of the function was used to obtain the angle, θ_α. In order to obtain a value for the numerical aperture of the the fiber, equation (3) was used. To measure the angular acceptance with Gaussian beam theory, i.e. the half-angle divergence, equation (8) was used together with the estimate for the beam diameter to approximate the beam's waist

radius, w_0. The acceptance angle obtained from the NA measurements, which is model based on geometrical optics, was compared to the half angle divergence calculate with Gaussian beam theory. Furthermore, to calculate the V-number, equation (4) was used and thus the approximate number of modes was obtained with equation (5).

2.4 Measurements of the Transmission Spectrum

The transmitted wavelengths of two 6.4 mm samples of the fabricated fiber were measured with a White-Light Laser and an Optical Spectral Analyzer (OSA). In the measured interval, 600 µm to 1750 µm, the absorbed wavelengths are about 730 nm and 800 nm. Since the relevant absorbed wavelengths by Nd:YAG are known, the obtained spectra of the fiber was examined for absorption peaks in order to estimate the presence of Nd in the core as an indicator of whether the core and the cladding had interfered with the core during the drawing process. Furthermore, the transmission spectra and more precisely which wavelengths are absorbed by the core is an important indicator of the fiber's quality as a reliable waveguide.

2.4.1 Experimental Configuration

The transmission spectrum of the fiber samples were measured in order to understand which wavelengths of light are transmitted through the core of the fiber and which are absorbed. The measurement was conducted using the same optical configuration as the measurements of the numerical aperture. Instead of a CCD-camera and a piece of paper, a multi-mode fiber cable was mounted on a translation stage, which was aligned with the fiber's core. The multi-mode fiber cable was connected to an optical spectral analyzer. An interval of wavelengths, 600 nm to 1750 nm and resolution of 1 nm of was chosen. There were three presets of power on the used laser, 25%, 50%, and 75%. The measurements were conducted on 50% power to maximize the the signal and minimize the noise. Four measurements were conducted in total and data sets with values for signal in units of dB m as a function of the wavelength (m) for each separate measurement were obtained.

The spectra were plotted for every measurement and compared to each other to examine whether the the absorption peaks matched.

A reference measurement was made with a 1wt% Nd:YAG rod used during the fiber drawing. In theory, the absorption peaks between the Nd:YAG rod and the fiber should match at the known wavelengths - 730 nm and 800 nm. The experimental configuration was similar. The single mode optical fiber (8 µm core) was connected to a 15mm 10x collimating lens, which was narrowing the beam going through a 1 wt% Nd:YAG rod (2 cm long and 1 mm in diameter). At the other end of the rod, the beam was going through an identical 15 mm 10x collimating lens in order to further narrow down the beam to going into a multi-mode optical fiber connected to the OSA. The multi-mode fiber was mounted on a translation stage to align the fiber with the laser beam.

2.5 Measurements of the Emission Spectrum

Another indication of the elemental composition of the fabricated fiber is its emission spectrum. The phenomena Amplified Spontaneous Emission was utilized by letting a beam from a 808 nm diode laser interact with a sample of the fiber. The emitted wavelengths by the Nd:YAG core are known and thus the experimentally obtained emission spectrum was compared with the known emission peaks.

2.5.1 Experimental Configuration

An integral part of the the experimental configuration was the diode laser which was connected with a single-mode optical fiber to a 8 mm collimating lens, which was coupled with another 2.8 mm collimating lens. The single-mode optical fiber from the laser was mounted to a translation stage in order to align the laser beam with the lenses and the studied fiber. After going through these two lenses, the beam was entering 6.4 mm sample of the studied fiber mounted on a translation stage used to align the fiber with the incoming laser beam. The fiber was connected to a multi-mode optical fiber also mounted on a translation to a align it with studied fiber. When aligning the single-mode

fiber connected to the laser and the studied fiber with the lenses, an IR-viewer was used to observe the laser beam as well as an IR-detector card for observing the spot from the laser beam. The multi-mode optical fiber was used to guide the incoming light from the fiber into an OSA to measure the emitted wavelengths by the YAG silica fiber's core. The OSA was centered at the known emission wavelengths (910 nm, 1064 nm, and 1400 nm) with a span of 100 nm and a resolution of 1 nm. The measurements were conducted on three different powers of the laser - 0.7 W, 1.4 W and 2.0 W.

2.6 Comparison with the Theoretical Optical Properties of the Fiber

The experimental measurements of the fiber's optical properties were compared to theory by using the previously measured refractive indices of the core and the cladding. The measured numerical aperture was also used to calculate the refractive index of the core to compare it with previous measurements of the refractive index of Nd:YAG.

2.6.1 Numerical Aperture, V-number, and Number of Modes

Using equation (3), the numerical aperture of the fiber was calculated with previously measured refractive indices for the core and the cladding. This value was compared to the experimentally measured value for the numerical aperture. The experimental numerical aperture was also used to calculate the refractive index of the Nd:YAG core and compare it to previously measured values.

Similarly, the theoretical and experimental V-numbers were calculated with equation (4). If the V-numbers were greater than 2.405, the number of modes was greater than one, these values could be used to approximate the number of modes in the fiber with equation (5).

3 Results

The dimensions and structure of the YAG silicate fiber were measured. In order to estimate the elemental composition of the fiber, the content of each element contained in silica and and Nd:YAG were compiled from the EDS measurements. The obtained transmission and emission spectra were used both as an estimate of the fiber's optical properties and an indication of its elemental composition, since the transmitted, absorbed, and emitted wavelengths are characteristic to the materials used in the fiber. The optical angular acceptance of the fiber was estimated by comparing the results from models based on geometrical optics and Gaussian beam theory.

3.1 Structural Properties

Structural measurements conducted with a microscope, showed that the fiber had a clear core and cladding, see figure 5. The diameter of the fiber was measured to be 127.1 ± 35.37 µm and the diameter of the core was measured to be 35.75 ± 6.37 µm (see Appendix A for the dataset from the measurements). However, the dimensions of the fiber were not uniform along the fiber and there were multiple structural imperfections. For instance, the core and the cladding were not uniformly cylindrical, as seen from the fiber's cross section in Figure 6a. Additionally, there were multiple parts of the fiber's core with no Nd:YAG present; see for instance the bubble in Figure 6b.

(a) End of the fiber, 20x. (b) Side of the fiber, 15x.

Figure 5: Microscope pictures of fiber.

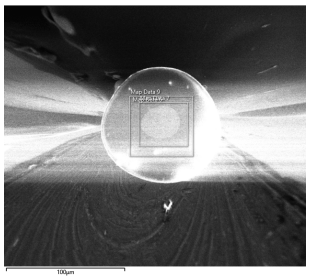

(a) SEM picture of the fiber's cross section

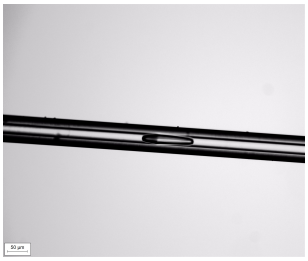

(b) An air bubble in the fiber's core, 20x.

Figure 6: Microscope pictures of fiber.

Furthermore, there were continuous sections of core with no Nd:YAG as well as parts of the core and the cladding with various tensions and stress present, such as in Figure 7.

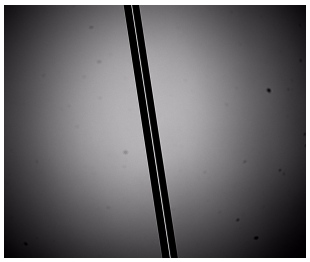

(a) Section of the fiber's core with no present Nd:YAG, 15x.

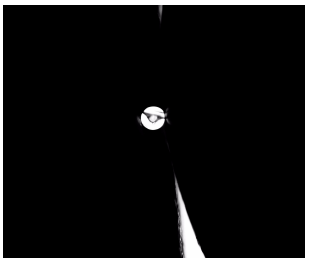

(b) Stressed end of the fiber, 15x.

Figure 7: Microscope pictures of fiber.

3.2 Elemental Composition

As seen in Figure 8a and 8b, there is a higher content of silicon and thus silica as well as oxygen in the cladding. Similarly, there is s a higher content of aluminum in the core, see Figure 8c. This indicates that the fundamental structure of the fiber was preserved.

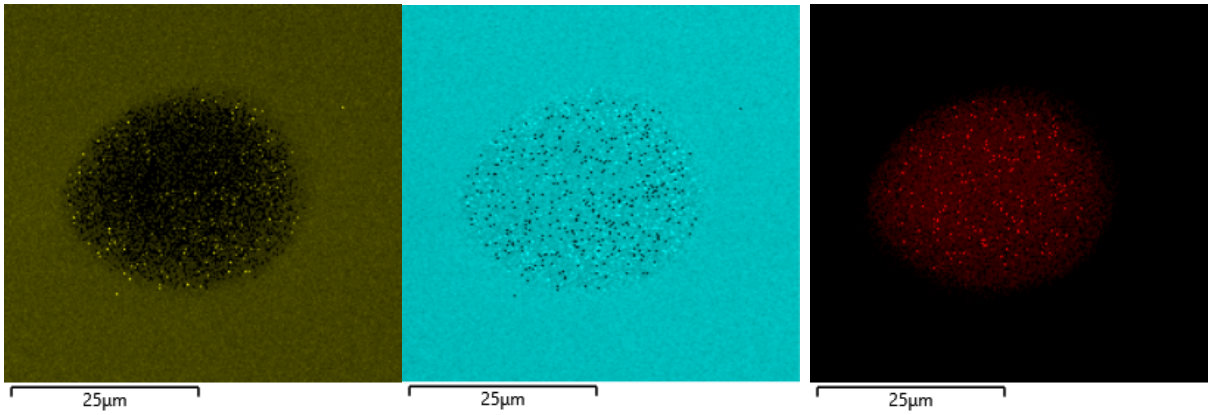

(a) Silicon content (b) Oxygen content (c) Aluminum content

Figure 8: EDS scan of the fiber's cross section; colored dots indicate the presence of the studied element.

The same conclusion can drawn from the data over the specific weight percentages of each element. From Figure 9, the average content silicon was determined to be $8.5 \pm 2.6\,\mathrm{wt\%}$ in the core and $30 \pm 7.9\,\mathrm{wt\%}$ in the cladding, which implies that the core contains significantly more Nd:YAG than previous studies.

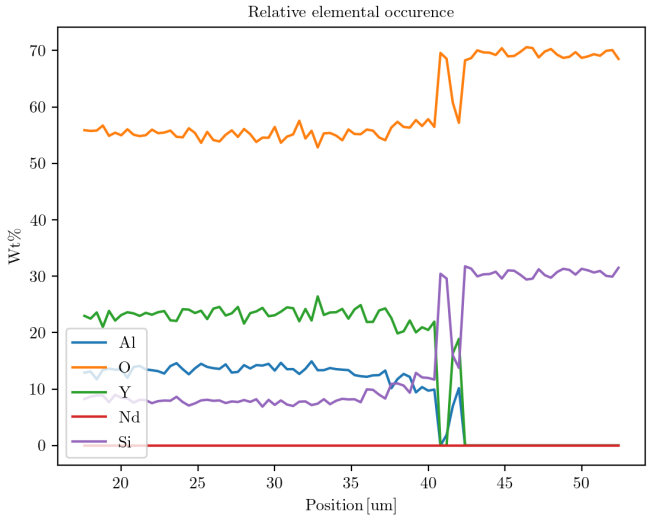

Figure 9: Weight percentages of each element as functions of distance.

Furthermore, it is clearly visible in Figure 9 that the content of elements characteristic for the silica in the cladding increases at about 41 µm.

3.3 Angular Acceptance, V-number, and Number of Modes

As seen in Figure 10, the width of the beam increase linearly with the distance of the CCD-camera from the laser spot. The value of the coefficient of determination, R^2 is 0.991, which means that the model explains 99.1% of the data in the linear regression model.

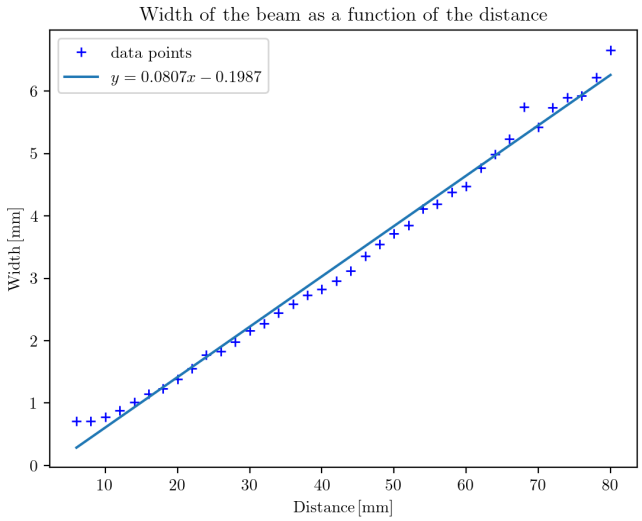

Figure 10: The width of the beam as a function of the distance.

Using slope of the linear function, the acceptance angle estimated to be 4.58° and thus the estimate value of the numerical aperture is 0.0805. Using equation (8) from the Gaussian beam theory, the half angle divergence is $0.60° \pm 0.0543°$. Using the numerical aperture, the refractive index of the core was to calculated to be 1.46. Furthermore, the V-number is 18.1 ± 3.21 and consequently the number of modes is approximated to 164 ± 58.3.

3.4 Transmission Spectra

As seen in Figure 12, the absorbed wavelengths are as predicted approximately 730 nm and 800 nm, which also approximately corresponds to the absorbed wavelengths for the Nd:YAG rod used as a reference.

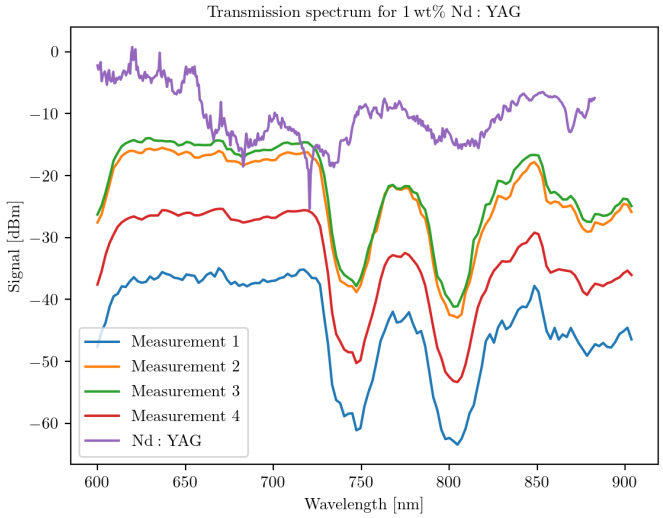

Figure 11: The transmission spectrum for 1 wt% Nd:YAG; local minima indicate absorption.

However, some deviations of the measured absorbed wavelengths by the YAG silica fiber's core and the reference Nd:YAG rod can be observed as wells a deviations from the previously measured wavelengths 730 nm and 800 nm.

3.5 Emission Spectra

As seen in Figure 12, the emitted wavelengths approximately correspond to 946 nm, 1064 nm, and 1338 nm.

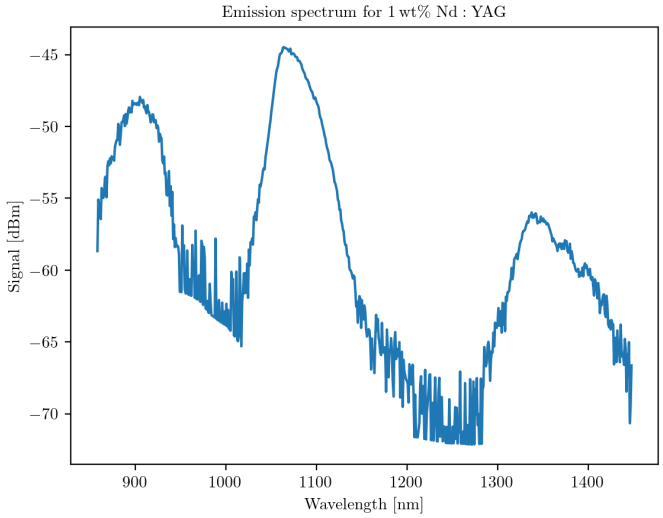

Figure 12: The emission spectrum for 1 wt% Nd:YAG; the peaks indicate emission.

There are, however, some deviations of the measured emitted wavelengths by the YAG silica fiber's core and the previous values for the emitted wavelengths (946 nm, 1064 nm, and 1338 nm) by Nd:YAG.

4 Discussion

As seen in in Figure 5, the base structure of the fiber was preserved with two approximately cylindrical layers in the form of the core and the cladding. The same conclusion can be drawn from the EDS scan of the fiber in Figure 8, where a higher content in the core of elements which are part of the YAG crystal can be observed. Additionally, the average content of silicon in the core was estimated to be 8.5 ± 2.6 wt% from Figure 9. In comparison with previous studies on YAG-derived fibers where the content of silicon was 75.3 wt%, the YAG silica fiber in this study has a higher content of Nd:YAG in the core. One possible reason, is the higher viscosity of silica than the one of YAG, which minimizes diffusion of the materials during the fabrication. Since silica has a higher thermal expansion coefficients than Nd:YAG, the temperature used and the time of heating is of importance. The fact that the fiber was heated for a longer period of time in previous

studies, could contribute to the higher content of Nd:YAG in the core region of the fiber.

However, the higher thermal expansion coefficient of YAG can also lead to a mixed composition as seen in Figure 9. Furthermore, a higher thermal expansion coefficient of Nd:YAG also implies faster thermal reduction during the cooling phase of the fabrication process, which also could also contribute to the mixed material composition of the fiber. Apart from the composition of materials, thermal expansion could possibly lead to a non-uniform core- structure and altered shape, which could affect the fibers optical properties by changing the angle of incidence for the light entering the fiber, potentially lead to the scattering of light and hence transmission losses. Additionally, when the two materials are in liquid forms, diffusion can also contribute to a varied material composition, even if the higher viscosity of silica decreases diffusion. When the bottom of the preform is in a liquid state and the other parts are in a solid state, the role of diffusion could be increased by the pulling force of gravity on the liquid parts of the preform [36].

The acceptance angle, θ_α, and the numerical aperture were estimated to be 4.58° and 0.0805 respectively [39]. From this the numerical aperture of the fiber's core was calculated to be 1.46, which deviates 25.5% from the previously measured value of 1.83. One reason for this deviation, could be mixed composition of the fiber's core, as seen in Figures 8 and 9. However, since geometrical optics utilizes the weak guidance approximation, i.e. some algebraic simplifications are made under the assumption that the difference between the refractive index of the core and the cladding, $\Delta n = n_{core} - n_{cladding}$, is small, typically less than 1 % [39]. In particular, the paraxial approximation is utilized for small Δn, which is a small angle approximation for the sine, cosine and tangent function. This implies that since the difference in refractive index (using previously measured values) is $\Delta n = 1.83 - 1.46 = 0.36$, which is more than 1%, the case of this fiber could be beyond the weak guidance approximation, making the conducted measurement inaccurate. This notion is further confirmed by the deviation from the half angle divergence calculated from Gaussian beam theory,

There were, however, additional sources of error in this study, associated with the

precision of the EDS measurements. As seen in Figure 9, the neodymium could not be detected with EDS, which could possibly be explained by the small of amounts of the neodymium used in the core (1 wt%), requiring higher precision. Another factor affecting the precision is that the energy of the focused beam optimized to detect middle-weight elements like silicon, aluminum and yttrium are not optimal for lighter elements like oxygen, which could make the measured content of oxygen inaccurate. Furthermore, since the emitted energy by oxygen is lower than the emitted energy by middle-weight elements, which means that the EDS could detect weaker low-energy stray signals as registering them as oxygen. Even in the absorbed and emitted wavelengths in Figure 11 and 12 were specific to Nd:YAG and thus indicated the presence of of neodymium, more detailed calibration could quantify the proportions of each element, including neodymium, more precisely. Another source of error is the presence of bubbles in the fiber's core as seen in 6b, affecting its optical properties by scattering the light. The reason for their presence lies in the fabrication process and there is a possibility that the surrounding air interacted with the fiber during the drawing process.

4.1 Conclusion

It can be concluded that the fabricated YAG silicate fiber in this study has a higher content of Nd:YAG in the core than in previous studies. The fabrication method used is thus deemed feasible for fabricating Nd:YAG optical fibers with a higher purity of the core materials. However, further studies are necessary in order to improve the method with respect to the thermal properties of the used materials, and to further increase the uniformity of the fiber's structure and the purity of the Nd:YAG in the core.

Furthermore, deviations of optical measurements for the angular acceptance of the fiber from theory and Gaussian beam models are an indication that the scenario of this fiber is beyond the weak guidance approximation used in models based on geometrical optics. Thus, future studies need to be conducted to improve the accuracy of angular acceptance measurements. Another potential area of interest for future studies, is the

viability of optical fibers with thermally similar materials to Nd:YAG in the core, such as other crystalline semiconductive compounds, coupled, for greater generality, with different dopants such as erbium, niobium, and thulium.

References

[1] Paschotta R. Fibers. In: Encyclopedia of Laser Physics and Technology. Wiley; 2008. Available from: https://www.rp-photonics.com/fibers.html.

[2] Augustyn A, Gaur A, Gregersen E. Refractive index. Encyclopædia Britannica;. Available from: https://www.britannica.com/science/refractive-index.

[3] Young HD, Freedman RA. Chapter 35. In: University Physics. Addison-Wesley series in physics. Addison-Wesley; 1996. Available from: https://books.google.se/books?id=YShBAQAAIAAJ.

[4] Snell's Law. Libretexts; 2021. Available from: https://eng.libretexts.org/Bookshelves/Materials_Science/Supplemental_Modules_(Materials_Science)/Optical_Properties/Snell's_Law.

[5] Total internal reflection. Libretexts; 2022. Available from: https://phys.libretexts.org/Bookshelves/College_Physics/Book%3A_College_Physics_(OpenStax)/25%3A_Geometric_Optics/25.04%3A_Total_Internal_Reflection.

[6] Paschotta R. Numerical Aperture. In: Encyclopedia of Laser Physics and Technology. Wiley; 2008. Available from: https://www.rp-photonics.com/numerical_aperture.html.

[7] Paschotta R. V Number. In: Encyclopedia of Laser Physics and Technology. Wiley; 2008. Available from: https://www.rp-photonics.com/v_number.html.

[8] Paschotta R. Gaussian Beams. In: Encyclopedia of Laser Physics and Technology. Wiley; 2008. Available from: https://www.rp-photonics.com/gaussian_beams.html.

[9] Self SA. Focusing of spherical Gaussian beams. Applied optics. 1983;22(5):658-61.

[10] Crystran. Silica Glass (SiO2) Optical Material — crystran.co.uk;. [Accessed 09-Jul-2022]. https://www.crystran.co.uk/optical-materials/silica-glass-sio2.

[11] Kupp E, Messing G, Anderson J, Gopalan V, Dumm J, Kraisinger C, et al. Co-casting and optical characteristics of transparent segmented composite Er:YAG laser ceramics. Journal of Materials Research - J MATER RES. 2010 03;25:476-83.

[12] Undoped Yttrium Aluminium Garnet (YAG) — mt-berlin.com;. [Accessed 12-Jul-2022]. http://www.mt-berlin.com/frames_cryst/yag_un.htm.

[13] Vorona IO, Yavetskiy RP, Doroshenko AG, Parkhomenko SV, Chernomorets EG, Tolmachev AV, et al. Reactive sintering of highly-doped YAG/Nd3+: YAG/YAG composite ceramics. Processing and Application of Ceramics. 2017;11(4):290-5.

[14] Paschotta R. Amplified Spontaneous Emission. In: Encyclopedia of Laser Physics and Technology. Wiley; 2008. Available from: https://www.rp-photonics.com/amplified_spontaneous_emission.html.

[15] Paschotta R. Spontaneous Emission. In: Encyclopedia of Laser Physics and Technology. Wiley; 2008. Available from: https://www.rp-photonics.com/spontaneous_emission.html.

[16] Paschotta R. Stimulated Emission. In: Encyclopedia of Laser Physics and Technology. Wiley; 2008. Available from: https://www.rp-photonics.com/stimulated_emission.html.

[17] Paschotta R. Population Inversion. In: Encyclopedia of Laser Physics and Technology. Wiley; 2008. Available from: https://www.rp-photonics.com/population_inversion.html.

[18] Paschotta R. Optical Pumping. In: Encyclopedia of Laser Physics and Technology. Wiley; 2008. Available from: https://www.rp-photonics.com/optical_pumping.html.

[19] Paschotta R. YAG Lasers. In: Encyclopedia of Laser Physics and Technology. Wiley; 2008. Available from: https://www.rp-photonics.com/yag_lasers.html.

[20] Wang X, Nie Q, Xu T, Liu L. A review of the fabrication of optic fiber. In: Breckinridge J, Wang Y, editors. ICO20: Optical Design and Fabrication. vol. 6034. International Society for Optics and Photonics. SPIE; 2006. p. 346 354. Available from: https://doi.org/10.1117/12.668147.

[21] Paschotta R. Fiber Fabrication. In: Encyclopedia of Laser Physics and Technology. Wiley; 2008. Available from: https://www.rp-photonics.com/fiber_fabrication.html.

[22] Mawardi A, Pitchumani R. Optical fiber drawing process model using an analytical neck-down profile. IEEE Photonics Journal. 2010;2(4):620-9.

[23] Agrawal G. Chapter 1. In: Nonlinear Fiber Optics. Elsevier Science; 2013. Available from: https://books.google.se/books?id=xNvw-GDVn84C.

[24] PubChem Compound Summary for CID 24261, Silicon dioxide.. U.S. National Library of Medicine;. Available from: https://pubchem.ncbi.nlm.nih.gov/compound/Silicon-dioxide.

[25] Yttrium Aluminium Garnet (YAG);. Available from: https://www.crystran.co.uk/optical-materials/yttrium-aluminium-garnet-yag.

[26] Ballato J, Peacock AC. Perspective: Molten core optical fiber fabrication—A route to new materials and applications. APL Photonics. 2018;3(12):120903.

[27] Doremus RH. Viscosity of silica. Journal of Applied Physics. 2002;92(12):7619-29.

[28] Silicon Dioxide Properties. Vienna University of Technology;. Available from: https://www.iue.tuwien.ac.at/phd/filipovic/node26.html.

[29] Bradbury S, Joy DC, Ford BJ. Scanning electron microscope. Encyclopædia Britannica; 2009. Available from: https://www.britannica.com/technology/scanning-electron-microscope.

[30] Goldstein NDE J, C JD. Scanning Electron Microscopy and X-Ray Microanalysis: Third Edition. Scanning Electron Microscopy and X-ray Microanalysis. Springer US; 2003. Available from: https://books.google.se/books?id=ruF9DQxCDLQC.

[31] Egdell RG, Bruton E. Henry Moseley, X-ray spectroscopy and the periodic table. Philosophical Transactions of the Royal Society A. 2020;378(2180):20190302.

[32] An Introduction to Energy Dispersive X-ray Spectrometry (EDS). 2010. Available from: https://www.sciencedirect.com/science/article/pii/S106852001000074X.

[33] Hosch WL, Young G. Auger effect. Encyclopædia Britannica, inc.; 1998. Available from: https://www.britannica.com/science/Auger-effect.

[34] Paschotta R. Silica Fibers. In: Encyclopedia of Laser Physics and Technology. Wiley; 2008. Available from: https://www.rp-photonics.com/silica_fibers.html.

[35] Ballato J, Hawkins T, Foy P, Yazgan-Kokuoz B, McMillen C, Burka L, et al. Advancements in semiconductor core optical fiber. Optical Fiber Technology. 2010;16(6):399-408. Special Fiber Structures and their Applications. Available from: https://www.sciencedirect.com/science/article/pii/S106852001000074X.

[36] Xie Y, Liu Z, Cong Z, Qin Z, Wang S, Jia Z, et al. All-fiber-integrated Yb: YAG-derived silica fiber laser generating 6 W output power. Optics express. 2019;27(3):3791-8.

[37] Dragic PD, Liu YS, Ballato J, Hawkins T, Foy P. YAG-derived fiber for high-power narrow-linewidth fiber lasers. In: Honea EC, Hendow ST, editors. Fiber Lasers IX: Technology, Systems, and Applications. vol. 8237. International Society for Optics and Photonics. SPIE; 2012. p. 248 256. Available from: https://doi.org/10.1117/12.907478.

[38] Dragic PD, Ballato J, Hawkins T, Foy P. Feasibility study of Yb:YAG-derived silicate fibers with large Yb content as gain media. Optical Materials. 2012;34(8):1294-8. Available from: https://www.sciencedirect.com/science/article/pii/S0925346712000900.

[39] Snyder AW, Love J. Optical waveguide theory. Springer Science & Business Media; 2012.

A Appendix A

Table 1: Dataset for the outer and inner diamter of the YAG silica fiber

d_{outer} [µm]	d_{inner} [µm]
135.81	36.66
100.27	31.41
135.34	34.44
147.65	40.11
111.24	36.12
132.21	35.55